Self-Consistent Cutoff Wave Number of the Ablative Rayleigh-Taylor Instability

The Rayleigh-Taylor instability occurs at the interface between heavy and light fluids when the heavy fluid is accelerated by the light fluid. The classical treatment[1] of a sharp interface shows that a small perturbation at this boundary will grow as $e^{\gamma t}$, where $\gamma = \sqrt{A_T kg}$ is the linear growth rate, k is the mode wave number, g is the acceleration, and

$$A_T = (\rho_h - \rho_l)/(\rho_h + \rho_l)$$

is the Atwood number (ρ_h and ρ_l are the heavy- and light-fluid densities, respectively). The ablation front of an inertial-confinement-fusion (ICF) imploding target is subject to this instability because the compressed target is accelerated by the low-density ablating plasma. If small perturbations caused by either target imperfections or illumination nonuniformity grew classically, they would grow to sufficient amplitude to destroy the shell of the target and degrade the performance of the implosion. However, because the shell material is ablated by the laser, the growth is reduced with respect to the classical value and, for sufficiently short wavelengths, the instability is suppressed.[2–12] Thus, only those modes with wave number k smaller than a critical value ($k < k_c$, where k_c is the cutoff wave number) are unstable.

The calculation of the cutoff wave number of the unstable spectrum has been previously attempted by several authors.[7,8,10] The most common analytic models of the Rayleigh-Taylor instability of laser-illuminated pellets consider inviscid and incompressible fluids. The incompressible model[7,8] is not self-consistent as the equilibrium and the perturbations are described by different equations. In this model, the equilibrium flow is compressible $(\nabla \cdot \mathbf{U} \neq 0)$, but the perturbation is assumed to be divergence-free $(\nabla \cdot \tilde{\mathbf{v}} = 0)$. The incompressibility condition leads to a fourth-order differential equation for the perturbation that can be analytically solved. In other models,[5,6] the assumption of a divergence-free perturbation has been removed by retaining the effects of finite thermal conductivity. However, because of the difficulties in determining the analytic solutions, a sharp-boundary model has been used in representing the equilibrium.[5] Such an approximation to the equilibrium is not self-consistent since the plasma density in the blowoff region cannot be approximated by a flat profile. Subsequently, the growth rate has been calculated using a sharp-boundary model for the perturbations and a diffuse density profile for the equilibrium.[11] The density jump across the ablation front is calculated by retaining the thermal conductivity, and the derived growth rate is in good agreement with Takabe's numerical results.[1] Nevertheless, such a model is still not self-consistent since the equilibrium and perturbed quantities satisfy different equations. A more accurate treatment of the effect of finite thermal conductivity in a diffuse density profile can be found in Ref. 9, where the growth rate of the instability is calculated semi-analytically by matching the analytic solution in the overdense region with the numerical solution in the blowoff region. The first truly analytical estimate of the cutoff wave number for direct-drive ICF without radiation effects ($\nu = 2.5$), including the effects of finite thermal conductivity, is derived in Ref. 10. In that work, the Wentzel-Kramers-Brillouin (WKB) approximation is used to determine the solution in the downstream region assuming that the mode wavelength is smaller than the density-gradient scale length and the cutoff wave number is derived by connecting that solution with the one in the upstream region.

It is noteworthy that numerical simulations of indirect-drive ICF capsule implosions have shown a different growth rate of the instability in comparison with direct drive. We attribute this difference to the mechanism of energy transfer that, in indirect-drive ICF, is dominated by radiation transport over electronic thermal conduction. According to the simple model of Ref. 13, the heat flux transported by radiation heat conduction is

$$\mathbf{q} = -(lc/3)\nabla U_p = -(lc/3)\nabla\left(4\sigma T^4/c\right),$$

where $U_p = 4\sigma T^4/c$ is the equilibrium radiation energy density and l is the Rosseland mean free path. The energy flux can be written in terms of the gradient of temperature and an effective radiation thermal conductivity $K = 16\sigma T^3 l/c$, where the radiation mean free path l is assumed to be proportional to some power of the temperature and density. Since the pressure-

gradient scale length is much larger than the density and temperature gradient scale length in the ablation front ($p \simeq$ const), the radiation heat conduction has a strong dependence on the temperature. Thus, it became clear that a cutoff wave number formula valid for a general thermal conduction law was needed. In this article, the formula for the cutoff is derived for an arbitrary power-law dependence of the thermal conductivity ($K \sim T^{\nu}$) with $\nu > 1$, and it can be applied to a wide class of equilibria described by different values of ν. The corresponding eigenfunction is found by performing a "boundary layer" analysis of the solution in different regions of the density profile. The asymptotic matching of the eigenfunction through the boundary layers leads to an eigenvalue equation for the cutoff wave number. The analytically derived formula for the cutoff wave number is in excellent agreement with the numerical results of Ref. 6 for $\nu > 1$.

The Model

We consider an ablatively accelerated fluid in steady state. In the frame of reference of the ablation front, the evolution of the mass density ρ and the velocity $\mathbf{v}$ are described by the isobaric model of Kull and Anisimov[5]

$$\frac{\partial \rho}{\partial t} + \nabla \cdot \rho \mathbf{v} = 0 \tag{1}$$

$$\rho\left(\frac{\partial \mathbf{v}}{\partial t} + \mathbf{v} \cdot \nabla \mathbf{v}\right) = -\nabla p + \rho g \tag{2}$$

$$\nabla \cdot \left(\mathbf{v} + L_0 V_a \frac{\nabla \xi}{\xi^{\nu+2}}\right) = 0, \tag{3}$$

where $\mathbf{g} = g\mathbf{e}_y (g < 0)$, $\xi = \rho/\rho_a$ is the density normalized to its peak value ρ_a, and L_0 is the typical length of the ablation front

$$L_0 \equiv \frac{\gamma_h - 1}{\gamma_h} \frac{AK_a}{\rho_a V_a}. \tag{4}$$

Here, K_a is the thermal conductivity at the peak density, $A = m_i/(1 + Z)$ is the average particle mass, and γ_h is the ratio of specific heats. The parameter L_0 can be related to the density-gradient scale length $L = \rho(d\rho/dy)^{-1}$. Following Ref. 6, the equilibrium density profile can be obtained by combining Eqs. (1) and (3) into a single first-order differential equation

$$\frac{d\xi}{dy} = \frac{1}{L_0} \xi^{\nu+1} (1 - \xi) \tag{5}$$

with the boundary condition $\xi(y \to \infty) = 1$. Equation (5) yields the density-gradient scale length $L = L_0/\left[\xi^{\nu}(1-\xi)\right]$, and its minimum value[6] is proportional to

$$L_0\left(L_{\min} = \left[(\nu + 1)^{\nu+1}/\nu^{\nu}\right] L_0\right).$$

Although Eq. (5) cannot be solved analytically, an approximate solution can be found in the proximity of the peak density ($\xi \approx 1$ or overdense region) and the blowoff region ($\xi << 1$):

$$\xi^{\text{heavy}} \approx 1 - e^{-y/L_0} \qquad \xi^{\text{blowoff}} \approx \left(\frac{-L_0}{\nu y}\right)^{1/\nu}. \tag{6}$$

Equation (6) shows that the density gradient is sharp near the peak density where $L \simeq L_0$ and becomes smooth in the blowoff region where $L \simeq -\nu y$ and $-y >> L_0$. It is important to observe that the density-gradient scale length is determined by the thermal conductivity coefficient, the mass ablation rate, and the exponent ν. The density profile becomes smoother as K_a or ν increases.

Linear Stability Analysis

Since the equilibrium depends on the spatial coordinate y only, the perturbation can be Fourier decomposed in the x direction; i.e. $Q_1 = \tilde{Q}(y) \exp(ikx + \gamma t)$ where $\gamma \to 0^+$ for wave numbers approaching the cutoff $\left(k \to k_c^-\right)$. The linearized conservation equations can be written in the following dimensionless form:

$$\left(\Gamma_a \xi + \partial_{\hat{y}}\right) \tilde{n} + \frac{\tilde{u}_y}{\hat{L}} \frac{\xi}{\epsilon_c} + \xi \hat{\nabla} \cdot \tilde{\mathbf{u}} = 0 \tag{7a}$$

$$\tilde{\pi} - i\left(\Gamma_a \xi + \partial_{\hat{y}}\right) \tilde{u}_x = 0 \tag{7b}$$

$$\left(\Gamma_a \xi + \partial_{\hat{y}} - \frac{1}{\epsilon_c \hat{L}}\right) \tilde{u}_y + \partial_{\hat{y}} \tilde{\pi} + \tilde{n}\left(\frac{\xi}{\epsilon_c Fr} - \frac{1}{\epsilon_c \hat{L}\xi}\right) = 0 \tag{7c}$$

$$\hat{\nabla} \cdot \tilde{u} - \epsilon_c \tilde{\nabla}^2 \tilde{\Phi} = 0, \tag{7d}$$

where

$Fr = V_a^2/|g|L_0$ is the Froude number, $\hat{y} = ky$, $\Gamma_a = -\gamma/kV_a$, $\hat{\nabla} = k^{-1}\nabla$, $\epsilon_c = k_c L_0$ (k_c is the cutoff wave number), $\hat{L} = L/L_0$, and

$$\tilde{n} = \frac{\tilde{\rho}}{\rho}; \quad \tilde{\mathbf{u}} = -\frac{\tilde{\mathbf{v}}}{V_a}; \quad \tilde{\pi} = \frac{\tilde{p}}{\rho_a V_a^2}; \quad \tilde{\Phi} = \frac{\tilde{\rho}}{\xi^{\nu+2}}. \tag{7e}$$

Equations (7a)–(7d) can be easily combined into a single fifth-order differential equation for the density perturbation:

$$\left[\partial_{\hat{y}}\left(\Gamma_a\xi + \partial_{\hat{y}}\right)\partial_{\hat{y}} - \left(\Gamma_a\xi + \partial_{\hat{y}}\right)\right]\epsilon_c\,\hat{L}$$

$$\left[\left(\Gamma_a\xi + \partial_{\hat{y}}\right)\tilde{\Phi}\,\xi^{\nu} + \epsilon_c\,\hat{\nabla}^2\tilde{\Phi}\right]$$

$$+\,\partial_{\hat{y}}\left(\Gamma_a\xi + \partial_{\hat{y}}\right)\left[\partial_{\hat{y}}\tilde{\Phi}\xi^{\nu} + \epsilon_c\,\hat{\nabla}^2\tilde{\Phi}\right]$$

$$+\,\epsilon_c\,\hat{\nabla}^2\tilde{\Phi} + \tilde{\Phi}\frac{\xi^{\nu+2}}{\epsilon_c\,Fr} = 0. \tag{8}$$

Here, $V_a > 0$ and $\Gamma_a \to 0^-$. Equation (8) is an eigenvalue equation for the cutoff wave number $k_c\left(\epsilon_c = k_c L_0\right)$. We focus on equilibria characterized by $Fr > 1$, $\nu > 1$, and we order $\epsilon_c \sim Fr^{\nu/1-\nu}$. The validity of this assumption will be verified later by the matching conditions for the eigenfunction. In ICF, the Froude number varies significantly according to the target acceleration and the thermal conduction law. For the set of equilibria parameters considered in Ref. 4, $5 < Fr < g$, and it can be significantly lower for the equilibria considered in Ref. 14. The eigenfunction must satisfy the boundary conditions of vanishing perturbation at infinity; i.e., $\tilde{\mathbf{v}}\left(\pm\infty\right) = 0$, $\tilde{p}\left(\pm\infty\right) = 0$, and $\tilde{\rho}\left(\pm\infty\right) = 0$. Because of the variable scale length of the eigenfunction, three regions have been identified (Fig. 63.25): the overdense region (heavy fluid), the ablation front, and the blowoff region.

1. The Overdense Region

In ICF capsule implosions, the overdense portion of the shell represents the heavy-fluid region where $\hat{y} \sim 1$, $\rho \simeq \rho_a$, $\xi = 1 - \exp\left(-\hat{y}/\epsilon_c\right) + O\left[\exp\left(-2\hat{y}/\epsilon_c\right)\right]$, and $L >> L_0$. In this region and to lowest order in $\exp\left(-\hat{y}/\epsilon_c\right)$, Eq. (8) reduces to a constant-coefficient fifth-order differential equation

$$\left(\partial_{\hat{y}}^2 - 1\right)\left(\Gamma_a + \partial_{\hat{y}}\right)$$

$$\left(\epsilon_c\,\partial_{\hat{y}}^2 - \partial_{\hat{y}} + \Gamma_a - \epsilon_c\right)\tilde{\Phi}^h \exp\left(\hat{y}/\epsilon_c\right) = 0, \tag{9}$$

where $\Gamma_a \to 0^-$ and the superscript h denotes the heavy-fluid region. The solution of Eq. (9) can be written in the following form:

$$\tilde{\Phi}^h = \left(a^h e^{-\hat{y}} + b^h e^{\alpha^-\hat{y}} + c^h e^{\hat{y}} + d^h e^{-\Gamma_a\hat{y}} + q^h e^{\alpha^+\hat{y}}\right)e^{-\hat{y}/\epsilon_c}, \tag{10}$$

where a^h, b^h, c^h, d^h, q^h are integration constants and

$$\alpha^{\pm} = \left[1 \pm \sqrt{1 + 4\,\epsilon\left(\epsilon - \Gamma_a\right)}\right]\Big/2\,\epsilon.$$

To satisfy the boundary conditions of vanishing perturbation for $\hat{y} \to +\infty$, $c_h = d_h = q_h = 0$ and Eq. (10) reduces to the simple form

$$\tilde{\Phi}^h = \left[a^h e^{-\hat{y}} + b^h e^{\left(1 - \sqrt{1+4\epsilon_c^2}\right)\hat{y}}\right]e^{-\hat{y}/\epsilon_c}. \tag{11}$$

It is important to observe that the incompressible theory $\left(\nabla\cdot\tilde{\mathbf{v}} = 0\right)$ yields only the sonic solution

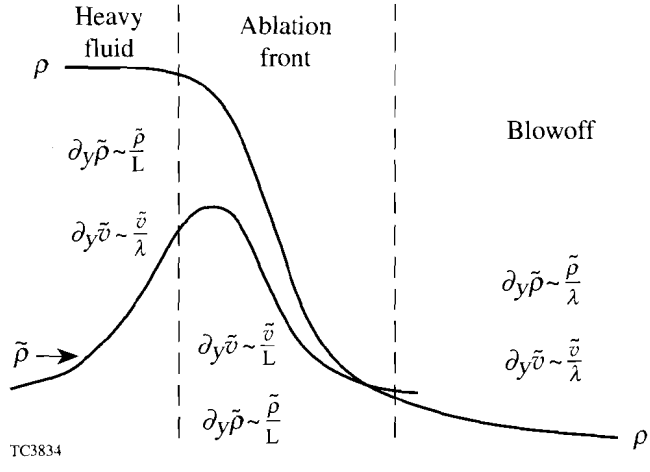

Fig. 63.25
Density profile with regions of different scale length of the perturbations. Here λ is the mode wavelength.

$$\tilde{\rho}^{\text{sonic}} \sim \exp\left[-\hat{y} - \hat{y}/\epsilon\right].$$

Equation (11) shows that a new solution is introduced by the finite thermal conductivity. Because of the diffusive character of thermal conduction, we denote the second term in Eq. (11) as the diffusion or entropy solution. Since the mode amplitude is arbitrary, we set $a_h + b_h = 1$, define the ablation front variable $z = \hat{y}/\epsilon_c$, and expand the solution for $z \sim 1$ and $\epsilon_c << 1$. A short calculation yields

$$\tilde{\Phi}^h = e^{-z}\left\{1-\left(1-b^h\right)\left[\epsilon_c\, z - \epsilon_c^2\,\frac{z^2}{2} + \epsilon_c^3\,\frac{z^3}{6} + O\left(\epsilon_c^4\right)\right] - \epsilon_c^2\, b^h z\right\}. \tag{12}$$

Each power of z in Eq. (12) needs to be matched to the ablation front solution.

2. The Ablation Front Region

The ablation front is the region where the density, velocity, and temperature profiles undergo a sharp variation. In this region, $\hat{y} \sim \epsilon_c$, $L \sim L_0$, and $\xi \sim 1$. Since $\xi \sim 1$, Eq. (5) cannot be solved in this region, and an explicit expression for the spatial dependence of the density profile cannot be found. Thus, it is more convenient to use ξ as the independent variable. By denoting with $\tilde{\Phi}^a$ the solution in the ablation region and after some straightforward manipulations, Eq. (8) can be rewritten in the following operator form:

$$\left(\mathcal{L}_0 + \epsilon_c^2\,\mathcal{L}_2 + \epsilon_c^3\,\mathcal{L}_3 + \epsilon_c^4\,\mathcal{L}_4\right)\tilde{\Phi}^a = 0, \tag{13}$$

where

$$\mathcal{L}_0 = \partial_z^3\left(\hat{L}\,\partial_z + 1\right)\left(\xi^\nu + \partial_z\right) \tag{13a}$$

$$\mathcal{L}_2 = -\partial_z^3\hat{L} - \partial_z\hat{L}\left(\partial_z\xi^\nu + \partial_z^2\right) \tag{13b}$$

$$\mathcal{L}_3 = \frac{\xi^{\nu+2}}{\epsilon_c\, Fr} \tag{13c}$$

$$\mathcal{L}_4 = \partial_z\hat{L} - 1. \tag{13d}$$

Here, $\partial_z = \xi^{\nu+1}(1-\xi)\partial_\xi$, $\hat{L} = \xi^{-\nu}/(1-\xi)$, and $z = \hat{y}/\epsilon_c$ is the ablation front coordinate ($z \sim 1$ in the ablation front region). We look for a solution of Eq. (13) in the form of an ϵ_c– series $\left(\hat{\Phi}^a = \sum_{j=0}^{\infty}\hat{\Phi}_j^a\,\epsilon_c^j\right)$, and we calculate all the terms up to third order in ϵ_c:

$$\mathcal{L}_0\hat{\Phi}_0^a = 0 \tag{14a}$$

$$\mathcal{L}_0\hat{\Phi}_1^a = 0 \tag{14b}$$

$$\mathcal{L}_0\hat{\Phi}_2^a = -\mathcal{L}_2\hat{\Phi}_0^a \tag{14c}$$

$$\mathcal{L}_0\hat{\Phi}_3^a = -\mathcal{L}_2\hat{\Phi}_1^a - \mathcal{L}_3\hat{\Phi}_0^a. \tag{14d}$$

Equation (14a) yields the following five homogeneous solutions:

$$\Psi_0 = \frac{1-\xi}{\xi} \qquad \Psi_1 = \frac{1-\xi}{\xi}z(\xi) \tag{15a}$$

$$\Psi_2 = \frac{1-\xi}{\xi}\left[\frac{z^2}{2} + \frac{1}{\nu}\int_1^\xi \frac{1+\nu\eta^\nu(\eta-1)-\eta^\nu}{\eta^{2\nu+1}(1-\eta)^2}\,d\eta\right] \tag{15b}$$

$$\Psi_3 = \frac{1-\xi}{\xi}\left[\frac{z^3}{6} - \int_1^\xi \frac{d\eta}{\eta^{\nu+1}(1-\eta)^2}\int_1^\eta z(\theta)\,\frac{1-\theta^{\nu+1}}{\theta^{\nu+1}}\,d\theta\right] \tag{15c}$$

$$\Psi_4 = \frac{1-\xi}{\xi}\int_{\xi_0}^\xi \frac{d\eta}{\eta^{\nu+1}(1-\eta)^2}, \tag{15d}$$

where the function $z(\xi)$ is derived from Eq. (5):

$$z(\xi) = \int_{\xi_0}^\xi \frac{d\tau}{\tau^{\nu+1}(1-\tau)} \tag{16}$$

(ξ_0 is the density at $z = 0$). Matching the zeroth and first-order solutions with the heavy-fluid solution yields $\tilde{\Phi}_0^a = \Psi_0$ and $\tilde{\Phi}_1^a = -\left(1-b^h\right)\Psi_1$. The second- and third-order equations [Eqs. (14c) and (14d)] are not homogeneous and require a combination of homogeneous and particular solutions to match the heavy-fluid solution. A long calculation leads to the following form of $\tilde{\Phi}_2^a$ and $\tilde{\Phi}_3^a$:

$$\tilde{\Phi}_2^a = \frac{1-\xi}{\xi}\frac{z^2}{2} - b^h\left(\Psi_1 + \Psi_2\right) \tag{17a}$$

$$\tilde{\Phi}_3^a = -\frac{1-\xi}{\xi}\left(1-b^h\right)\frac{z^3}{6} - \frac{1-\xi}{\xi}\int_1^\xi \frac{d\theta}{\theta^{\nu+1}(1-\theta)^2}\int_1^\theta ds$$

$$\times \int_1^s dx\, \frac{1-x^\nu}{x^{2\nu+1}(1-x)}\left[\frac{1}{\nu\,\epsilon_c\, Fr} + \frac{1-b^h}{\nu+1}\frac{1}{x}\right]. \tag{17b}$$

3. The Blowoff Region

The light-fluid or blowoff region is located downstream with respect to the ablation front. In this region, $-\hat{y} \sim 1$, $L >> L_0$, and $\xi \simeq \left(-L_0/\nu y\right)^{1/\nu} << 1$. The analysis can be simplified by introducing the new variable $\varsigma = \epsilon_c/\nu\,\xi^\nu$ and rewriting Eq. (8) in the following form:

$$M\tilde{\Phi}^l = 0, \tag{18a}$$

where

$$M = \partial_{\hat{y}}^4 + \partial_{\hat{y}}^3\frac{1}{\nu\varsigma} - 1 + \partial_{\hat{y}}\hat{\nabla}^2\frac{\nu\varsigma}{1-\xi}\left(\partial_{\hat{y}}\frac{1}{\nu\varsigma} + \hat{\nabla}^2\right) + \frac{1}{\nu\,\epsilon_c\, Fr}\left(\frac{\epsilon_c}{\nu}\right)^{2/\nu}\frac{1}{\varsigma^{1+2/\nu}}. \tag{18b}$$

Here, $\partial_{\hat{y}} = -\left(1-\xi\right)\partial_\varsigma$ and $\xi = \left(\epsilon_c/\nu\varsigma\right)^{1/\nu}$. Equation (18a) cannot be analytically solved for arbitrary ν. However, since $\nu > 1$ for both direct- and indirect-drive ICF, one could attempt to solve Eq. (18a) by performing a $1/\nu$ expansion of the operator and eigenfunction. Such an approach is reasonable for radiation-dominated transport in a fully ionized plasma as described in Ref. 13 ($\nu \sim 5$–8) but less convincing for electronic transport with $\nu = 2.5$. Thus, to check the validity of the expansion, we compare the analytical solution with the numerical results for $\nu = 2.5$. Based on that comparison, we deduce whether or not the $1/\nu$ expansion is a valid approach to the solution of Eq. (18a) in the regimes of interest for direct-drive ICF.

The next step is to rewrite the operator M and the eigenfunction $\tilde{\Phi}^l$ as power series in $1/\nu$:

$$M = \sum_{n=0}^{\infty} M_n\left(\frac{1}{\nu}\right)^{n-1} \tag{19}$$

$$\tilde{\Phi}^l = \sum_{n=0}^{\infty} \tilde{\Phi}_n^l\left(\hat{y}\right)\left(\frac{1}{\nu}\right)^n. \tag{20}$$

Substituting Eqs. (19) and (20) into Eq. (18a) and collecting terms up to the first two orders in $1/\nu$ leads to the following equations:

$$\partial_{\hat{y}}\left(\partial_{\hat{y}}^2 - 1\right)\varsigma\left(\partial_{\hat{y}}^2 - 1\right)\tilde{\Phi}_0^l = 0 \tag{21a}$$

$$\partial_{\hat{y}}\left(\partial_{\hat{y}}^2 - 1\right)\varsigma\left(\partial_{\hat{y}}^2 - 1\right)\tilde{\Phi}_1^l + \left[\left(1-\delta\right)\left(\partial_{\hat{y}}^4 - 1\right) + \partial_{\hat{y}}\left(\partial_{\hat{y}}^2 - 1\right)\varsigma\partial_{\hat{y}}\frac{1}{\varsigma} - \frac{\delta}{1-\delta}\partial_{\hat{y}}\left(\partial_{\hat{y}}^2 - 1\right)\varsigma\ln\varsigma\left(\partial_{\hat{y}}^2 - 1\right)\right]\tilde{\Phi}_0^l = 0, \tag{21b}$$

where $\delta = \left(\epsilon_c/\nu\right)^{1/\nu}$. We first solve the lowest-order equation [Eq. (21a)]. The solution of Eq. (21a) that satisfies the boundary conditions of vanishing perturbations at infinity can be written as a linear combination $\left[\tilde{\Phi}_0^l = A^l\tilde{\Phi}_A^l + B^l\tilde{\Phi}_B^l + C^l\tilde{\Phi}_C^l\right]$ of the following homogeneous decaying solutions:

$$\tilde{\Phi}_A^l = e^{\hat{y}} \qquad \tilde{\Phi}_B^l = e^{-\hat{y}}\int_{-\infty}^{\hat{y}} dx e^{2x}\int^x \frac{d\eta}{\varsigma(\eta)} \tag{22a}$$

$$\tilde{\Phi}_C^l = e^{\hat{y}}\int_o^{\hat{y}} dx e^{-2x}\int_{-\infty}^x d\eta\,\frac{e^{2\eta} - e^{\eta}}{\varsigma(\eta)}. \tag{22b}$$

(Note that in the light-fluid region $-\infty < \hat{y} < 0$.) To determine the constants of integration (A^l, B^l, C^l), the solution in the ablation front must be asymptotically matched to the solution in the light-fluid region. To perform the matching of the eigenfunction, it is necessary to expand the ablation front solution in powers of ($1/\nu$). A short calculation yields

$$\tilde{\Phi}^a = \frac{1-\delta}{\delta} + \frac{1}{\nu}\frac{\ln\varsigma}{\delta} + \frac{\varsigma}{\delta}\left(1-b^h\right)\left[1+\frac{1}{\nu}\left(\ln\varsigma + \frac{\delta}{1-\delta}\right)\right]$$

$$+ \frac{\varsigma^2}{2(1-\delta)^2}\left\{\frac{1-\delta}{\delta} + \frac{1}{\nu}\left[2-b^h + \left(\frac{1}{\delta}-2\right)\ln\varsigma\right]\right\}$$

$$+ \frac{\varsigma^3\left(1-b^h\right)}{6\delta(1-\delta)^2}\left\{1+\frac{1}{\nu}\left[\frac{1+5\delta+2\ln\varsigma(1-3\delta)}{2(1-\delta)}\right.\right.$$

$$\left.\left. + \frac{\delta\left(1-b^h\right)^{-1}}{2\,\epsilon_c\, Fr}\right]\right\} + O\left(\frac{1}{\nu^2}\right). \qquad (23)$$

Matching the lowest power of $1/\nu$ yields $A^l = (1-\delta)/\delta$, $B^l = 0$, and $C^l = 0$. The next step is to determine the first-order correction to $\tilde{\Phi}^l$ by substituting $\tilde{\Phi}_0^l$ into Eq. (21b) and solving for $\tilde{\Phi}_1^l$. Combining $\tilde{\Phi}_0^l$ and $\tilde{\Phi}_1^l$ gives the solution of the light-fluid equation up to first order in $1/\nu$:

$$\tilde{\Phi}^l \simeq \frac{1-\delta}{\delta} e^{\hat{y}}\left(1+\frac{1}{\nu}\frac{\ln\varsigma}{1-\delta}\right) + \frac{1-\delta}{\nu} C_1^l\, \tilde{\Phi}_C^l, \qquad (24)$$

where C_1^l is determined by matching Eq. (24) with the ablation front solution [Eq. (23)]. To perform the matching, we rewrite $\tilde{\Phi}^l$ for $\varsigma \to 0$:

$$\tilde{\Phi}^l(\varsigma\to 0) \simeq \frac{1-\delta}{\delta} + \frac{1}{\nu}\frac{\ln\varsigma}{\delta}$$

$$- \frac{\varsigma}{\delta}\left\{1+\frac{1}{\nu}\left[\ln\varsigma + \frac{\delta}{1-\delta}\left(1-C_1^l\ln 2\right)\right]\right\}$$

$$+ \frac{\varsigma^2}{2(1-\delta)^2}\left\{\frac{1-\delta}{\delta}\right.$$

$$\left. + \frac{1}{\nu}\left[1-C_1^l + \left(\frac{1}{\delta}-2\right)\ln\varsigma\right]\right\}$$

$$+ \frac{\varsigma^3}{6(1-\delta)^3}\left\{-\frac{1-\delta}{\delta} + \frac{1}{\nu}\left[C_1^l\left(\ln 2 + \frac{1}{2}\right) - 3\right.\right.$$

$$\left.\left. + \left(3-\frac{1}{\delta}\right)\ln\varsigma\right]\right\} + O\left(\varsigma^4\right). \qquad (25)$$

Matching equal powers of $1/\nu$ in Eqs. (23) and (25) leads to the following relations:

$$C_1^l = b^h = 2\left(1 - \frac{\ln 2}{\nu}\frac{\delta}{1-\delta}\right) \qquad (26)$$

$$\frac{1}{\epsilon_c\, Fr} \simeq \left(\frac{\epsilon_c}{\nu}\right)^{-1/\nu} + 2\left[1-\left(\frac{\epsilon_c}{\nu}\right)^{1/\nu}\right]^{-1}. \qquad (27)$$

In Eq. (27) all the terms up to first order in $1/\nu$ are retained. Higher-order terms in $1/\nu$ can be derived by solving Eq. (18a) to next order in $1/\nu$ and matching the solution with the $1/\nu$ expansion of the ablation front solution.[15] Using the results of Ref. 15, Eq. (27) can be rewritten in the following form:

$$\epsilon_c = \frac{\mu_0(\nu)}{Fr}\,\epsilon_c^{1/\nu}\, A_T(\epsilon_c) \qquad A_T(\epsilon_c) = \frac{1-\mu_0(\nu)\,\epsilon_c^{1/\nu}}{1+\mu_0(\nu)\,\epsilon_c^{1/\nu}}. \qquad (28)$$

Here, $\mu_0(\nu) = (2/\nu)^{1/\nu}/\Gamma(1+1/\nu)$, $\epsilon_c = k_c L_0$, and A_T is an effective Atwood number depending on the mode wavelength.

Discussion

The physical interpretation of the Atwood number in Eq. (28) is straightforward and may help to resolve the controversy about the right value of A_T to be used in the growth rate formulas. The classical definition of the Atwood number for a heavy fluid of constant density ρ_h superimposed on a light fluid of constant density ρ_l is $A_T = (\rho_h - \rho_l)/(\rho_h + \rho_l)$. However, for a monotonic diffuse density profile, the appropriate definition is $A_T = (\rho^+ - \rho^-)/(\rho^+ + \rho^-)$, where ρ^+ and ρ^- are the fluid densities calculated at some points where the eigenfunction is evanescent. For long-wavelength modes ($\epsilon_c = k_c L_0 << 1$), the eigenfunction for $\tilde{v}$ decays exponentially $\tilde{v} \sim e^{-k|y|}$ and becomes evanescent at a distance d of some wavelengths λ from the peak $y = 0$ ($d = \theta\lambda$, where θ is a constant of order unity). Thus, the Atwood number should be defined by setting $\rho^+ = \rho(d)$ and $\rho^- = \rho(-d)$. Using the equilibrium density profile $\rho = \xi\rho_a$ yields

$$\rho(d) = \rho_a + O\left(e^{-1/\epsilon_c}\right)$$

and

$$\rho(-d) \simeq \rho_a(\epsilon_c/\nu)^{1/\nu}/(2\pi\theta)^{1/\nu},$$

and the Atwood number of Eq. (28) is recovered by choosing $\theta = 1/2\pi\nu\mu_0^{\nu}$. It is important to observe that Eq. (28) can also be obtained by balancing the classical growth rate $\gamma_{cl} = \sqrt{A_T(\in)kg}$ with an effective ablation damping $\gamma_{ab} = -kV_{\text{eff}}$, where V_{eff} is the geometric average of the ablation velocity evaluated at distances d and $-d$ from the peak of the eigenfunction, $V_{\text{eff}} = \sqrt{V(d)V(-d)}$. Setting $\gamma = \gamma_{cl} + \gamma_{ab} = 0$ yields Eq. (28) for the cutoff wave number.

To test the validity of the $1/\nu$ expansion, we compare the cutoff wave number obtained by solving Eq. (28) with the numerical results available in the literature. Figure 63.26 shows a plot of the normalized cutoff wave number $k_c V_a^2/g$ versus the inverse Froude number. The solid line represents the solution of Eq. (28), and the dashed-dotted line represents the numerical results of Ref. 6 for $\nu = 2.5$. The remarkable agreement shown in Fig. 63.26 implies that the $1/\nu$ expansion is quite accurate even for $\nu = 2.5$. The disagreement in the regime of $Fr << 1$ is due to higher-order $\in_c$ corrections that become important for modes with wavelength shorter than the thickness of the ablation front. Figure 63.27 shows a plot of the normalized cutoff wave number versus ν for $Fr = 5$. The solid line represents the solution of Eq. (28) and the dots are the numerical results of Ref. 6. Observe the excellent agreement between the analytic and numerical results even in the region $\nu \sim 1$.

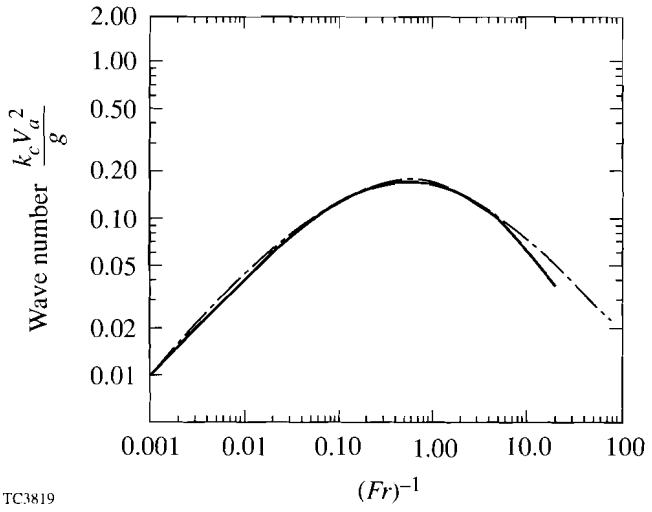

Fig. 63.26
Comparison of the normalized cutoff wave number $(k_c V_a^2/g)$ obtained from Eq. (28) (solid line) with the numerical results of Ref. 6 (dashed-dotted line).

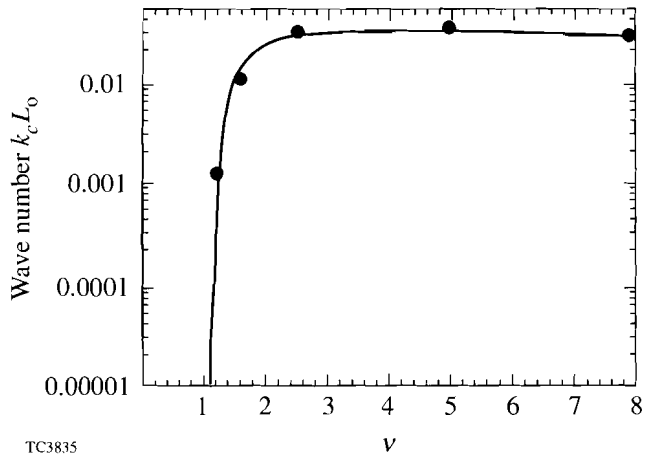

Fig. 63.27
Plot of normalized cutoff wave number $k_c L_0$ versus ν for $Fr = 5$. The solid line represents the solution of Eq. (28) and the dots are the numerical results of Ref. 6.

For electronic thermal conduction $\nu = 2.5$ and Eq. (28) can be compared with the analytic estimate of Ref. 10 that can be written in the following form:

$$\in_c = \frac{\in_c^{2/5}}{Fr}\,\frac{1-\in_c^{2/5}}{1+\in_c^{2/5}}. \tag{29}$$

Observe that Eq. (29) differs from Eq. (28) by terms $\mu_0(2.5)$. Since $\mu_0(2.5) = 1.03$, Eqs. (28)–(29) yield very similar results for electronic heat conduction. However, when diffusive radiation transport[13] dominates over electronic heat conduction, the thermal conductivity has a strong dependence on the temperature ($\nu \sim 5$–8) and Eq. (29) is not valid. In this case, the general formula (valid for arbitrary $\nu > 1$) derived in this article must be used to calculate the cutoff wave number. According to Ref. 13, $\nu = 6.5$ for a fully ionized gas; Fig. 63.28 shows the corresponding normalized cutoff wave number as a function of the inverse Froude number obtained by solving Eq. (28). We recognize that an accurate estimate of the cutoff wave number requires a more complete model of thermal conduction than the one described here. A multigroup treatment of the diffusive transport, as adopted in sophisticated codes such as *LASNEX*,[16] would probably lead to a more accurate result than the one of Eq. (28). Nevertheless, by judiciously choosing the values of ν and L_0, it is possible to fit

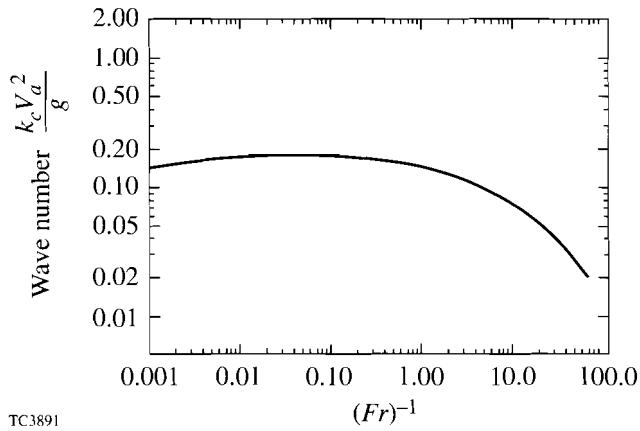

Fig. 63.28
Plot of the normalized cutoff wave number $\left(k_c V_a^2/g\right)$ obtained from Eq. (28) for $\nu = 6.5$ as a function of the inverse Froud number.

the equilibrium density profile obtained in the numerical simulations with the solution of Eq. (5). Obviously, different equilibria require different values of ν and L_0. Using such values in Eq. (28) should produce a reliable formula for the cutoff wave number with the appropriate values of the Atwood number and the ablative stabilization term.

To simplify the use of Eq. (28), the scale length L_0 is related to the distance L_e between the peak density and the $1/e$ point. The latter is the characteristic scale length widely reported in the literature. The isobaric model used here does not produce a maximum in the density and, in the overdense region, the density profile approaches the maximum value at infinity. Nevertheless, one can define an equivalent length as the distance between the point where the density is $\xi = 1/e$ and the point where the density is $\xi = \xi_0$, where $\xi_0 = 0.95$. A different choice of ξ_0 such as $\xi_0 = 0.99$ or $\xi_0 = 0.999$ would only slightly change the results as the density becomes exponentially flat in the overdense region. To determine L_e, the density profile is implicitly calculated by using Eq. (16), where $z = y/L_0$ and $\xi_0 = 0.95$. The integration in Eq. (16) can be carried out for integer or half-integer values of ν. A short calculation yields

$$\frac{L_e}{L_0} = z\left(\frac{1}{e}\right) = \sum_{i=0}^{m} \frac{e^{\nu-i}}{\nu-i}$$

$$+\ln\frac{\sqrt{\xi_0}\left(\sqrt{e}-1\right)}{\left(1-\sqrt{\xi_0}\right)} \qquad (\nu = n,\ m = n-1); \qquad (30)$$

$$\frac{L_e}{L_0} = z\left(\frac{1}{e}\right) = \sum_{i=0}^{m} \frac{e^{\nu-i}}{\nu-i}$$

$$+\ln\frac{2\sqrt{\xi_0}\left(\sqrt{e}-1\right)}{\left(\sqrt{e}+1\right)\left(1-\sqrt{\xi_0}\right)} \qquad (\nu = n+1\ 2, m = n). \qquad (31)$$

Equation (31) yields $L_e \simeq 14\ L_0$ and $L_e \simeq 190\ L_0$ for $\nu = 2.5$ and $\nu = 6.5$, respectively. Lastly, we compare the cutoff wave number derived here with the one produced by the incompressible theory of long-wavelength modes ($kL << 1$) or sharp boundary models.[2,17] These non-self-consistent derivations lead to growth rates of the form $\gamma = \sqrt{A_T kg} - \beta k V_a$, where $A_T = \left(\rho_h - \rho_l\right)/\left(\rho_h + \rho_l\right)$ is the Atwood number for flat profiles and $\beta = 1$ or 1.5. By setting $\gamma = 0$, the incompressible model yields a cutoff wave number $\epsilon_c = A_T/\left(\beta^2 Fr\right)$, quite different from the one satisfying Eq. (28).

Conclusions

The cutoff wave number of the ablative Rayleigh-Taylor instability is calculated self-consistently for an arbitrary power-law dependence of the thermal conductivity ($K \sim T^{\nu}$). The cutoff formula is valid for $\nu > 1$ and $Fr = V_a^2/gL_0 > 1$. Here V_a, g, and L_0 are the ablation velocity, the target acceleration, and the typical thickness of the ablation front, respectively. The derivation is carried out by expanding the eigenvalue equation in powers of $1/\nu$ and $\epsilon = kL_0$ and by performing a boundary layer analysis and asymptotic matching of the eigenfunction. The validity of the formula has been tested with the numerical solution of Ref. 6 up to values of ν close to 1, and the formula can be used for those equilibria (such as in indirect-drive ICF) that cannot be described by electronic heat conduction ($\nu = 2.5$ and $Fr \sim 5$).

ACKNOWLEDGMENT

This work was supported by the U.S. Department of Energy Office of Inertial Confinement Fusion under Cooperative Agreement No. DE-FC03-92SF19460, the University of Rochester, and the New York State Energy Research and Development Authority. The support of DOE does not constitute an endorsement by DOE of the views expressed in this article. Some of this work was carried out at the Institute for Theoretical Physics of the University of California at Santa Barbara, where the support of Prof. S. Cowley and the National Science Foundation (Grant No. PHY94-07194) is acknowledged.

REFERENCES

1. Lord Rayleigh, *Scientific Papers* (Cambridge University Press, Cambridge, England, 1900), Vol. II, pp. 200–207.

2. S. Bodner, Phys. Rev. Lett. **33**, 761 (1974).

3. C. P. Verdon, R. L. McCrory, R. L. Morse, G. R. Baker, D. I. Meiron, and S. A. Orszag, Phys. Fluids **25**, 1663 (1982).

4. H. Takabe, K. Mima, L. Montierth, and R. L. Morse, Phys. Fluids **28**, 3676 (1985).

5. H. J. Kull and S. I. Anisimov, Phys. Fluids **29**, 2067 (1986).

6. H. J. Kull, Phys. Fluids B **1**, 170 (1989).

7. A. B. Bud'ko and M. A. Liberman, Phys. Fluids B **4**, 3499 (1992).

8. R. Betti, V. Goncharov, R. L. McCrory, E. Turano, and C. P. Verdon, Phys. Rev. E **50**, 3968 (1994).

9. J. Sanz, Phys. Rev. Lett. **73**, 2700 (1994).

10. V. V. Bychkov, S. M. Golberg, and M. A. Liberman, Phys. Plasmas **1**, 2976 (1994).

11. J. G. Wouchuk and A. R. Piriz, Phys. Plasmas **2**, 493 (1995).

12. K. O. Mikaelian, Phys. Rev. A **46**, 6621 (1992).

13. Ya. B. Zel'dovich and Yu. P. Raizer, *Physics of Shock Waves and High-Temperature Hydrodynamic Phenomena* (Academic Press, NY, 1966), p. 152.

14. S. V. Weber, B. A. Remington, S. A. Haan, B. G. Wilson, and J. K. Nash, Phys. Plasmas **1**, 3652 (1994).

15. R. Betti, V. N. Goncharov, C. P. Verdon, and R. L. McCrory (in press).

16. G. B. Zimmerman and W. L. Kruer, Comments Plasma Phys. Controlled Fusion **11**, 51 (1975).

17. R. Betti, R. L. McCrory, and C. P. Verdon, Phys. Rev. Lett. **71**, 3131 (1993).